

GRAPHENE- AND GRAPHITE OXIDE-REINFORCED MAGNESIUM OXYCHLORIDE CEMENT COMPOSITES FOR THE CONSTRUCTION USE

ANNA-MARIE LAUERMANNOVÁ*, MICHAL LOJKA*, MILENA PAVLÍKOVÁ**, ADAM PIVÁK**,
MARTINA ZÁLESKÁ**, ZBYŠEK PAVLÍK**, OLDŘICH ZMEŠKAL***, #ONDŘEJ JANKOVSKÝ*

*Department of Inorganic Chemistry, Faculty of Chemical Technology, University of Chemistry and Technology,
Technická 5, 166 28 Prague 6, Czech Republic

**Department of Materials Engineering and Chemistry, Faculty of Civil Engineering, Czech Technical University in Prague,
Thákurova 7, 166 29 Prague 6, Czech Republic

***Faculty of Chemistry, Brno University of Technology, 612 00 Brno, Czech Republic

#E-mail: Ondrej.Jankovsky@vscht.cz

Submitted August 14, 2020; accepted October 20, 2020

Keywords: Graphene, Composites, Magnesium oxychlorides

Graphene and graphite oxide reinforced magnesium oxychloride cement (MOC) pastes were researched. To produce MOC pastes, the light-burnt magnesium oxide was added and dispersed in the magnesium chloride solution. The graphene powder, graphite oxide powder, and their combination were incorporated in the solution. The total amount of the nano additives was 0.5 % by the weight of the magnesium oxychloride binder. The morphology and microstructure of the hardened materials were studied using scanning electron microscopy (SEM). The phase composition of precipitated MOC-based products was investigated using X ray diffraction (XRD). The macrostructural parameters of the composites such as bulk density, specific density, and open porosity were evaluated. Mechanical strength and stiffness were analyzed by the measurement of flexural and compressive strength and dynamic elastic modulus. The electrical properties were examined by the use of impedance spectroscopy (IS). From the experimental results the model of the transport of electric charge in researched materials dispersion was estimated. The use of graphene- and graphite oxide-reinforcement of MOC matrix gave highly dense materials of low porosity, high mechanical resistance, whereas the used nano-additives enabled the produce of composites of high strength efficiency index. The addition of graphene particles and the formation of graphite agglomerates significantly decreased electrical resistivity of the MOC matrix which was originally characterized by low electrical conductivity.

INTRODUCTION

Magnesium oxychlorides (MOC), also known as Sorel cements, are a promising alternative to Portland cement (PC). They are inorganic compounds which form in the system $\text{MgO}-\text{MgCl}_2-\text{H}_2\text{O}$ by the reaction in the suspension of magnesium oxide powder dispersed in the aqueous solution of magnesium dichloride [1]. There are typically four types of such material. Their formation depends on the molar ratio of the precursors, temperature and reactivity of used magnesia powder. Depending on these conditions, either Phase 3 ($3\text{MgO}\cdot\text{MgCl}_2\cdot 8\text{H}_2\text{O}$) or Phase 5 ($5\text{MgO}\cdot\text{MgCl}_2\cdot 8\text{H}_2\text{O}$) can be obtained at laboratory temperature, and Phase 2 ($2\text{MgO}\cdot\text{MgCl}_2\cdot 4\text{H}_2\text{O}$) and Phase 9 ($9\text{MgO}\cdot\text{MgCl}_2\cdot 5\text{H}_2\text{O}$) can be obtained at temperatures above 100 °C [2-7]. The MOCs have an enormous potential as an alternative to Portland cement in terms of their environmental sustainability and their ability to capture CO_2 from the atmosphere. Their production is accompanied with a smaller amount of released CO_2 (compared to the

production of PC). Because of both reasons mentioned above, they can be marked as CO_2 -neutral [8-10]. They have very specific mechanical and other properties that are, in some ways, making them superior to PC. Namely, it is their very high fire-resistance[11], abrasion resistance[12], low rate of heat transport, and great elastic and acoustic properties [13]. These properties show the high potential of MOC in the construction industry. However, in previous studies, there were shown some difficulties with this sort of material, mostly with its low resistance to water. When exposed to water for a longer time, the magnesium chloride starts to leach from the structure. The primary structure of the binder is changing and the only compound left as a binding phase is brucite ($\text{Mg}(\text{OH})_2$) [14]. This problem was previously studied and there are multiple ways to minimize this drawback already presented in the literature [15-19]. One of the possible solutions to this problem is the addition of carbon-based nanomaterials in small percentages [20].

Graphene and graphite oxide belong to the group of carbon-based nanomaterials. They have very specific

chemical, physical and mechanical properties [21-24]. They can be divided into groups in terms of their dimensions. For example, buckminsterfullerene can be assigned to the group of 0D carbon nanomaterials, while carbon nanotubes (SWCNTs and MWCNTs) and graphene nanoribbons belong in the group of 1D nanomaterials and graphene and its derivatives such as graphene, fluorographene or graphene oxide are representatives of 2D carbon nanomaterials [25-27].

Graphene is mostly used in electronics, mainly because of its unique electronic, thermal and mechanical properties [28, 29]. However, as it is a zero-gap semiconductor, its possible applications are limited and it has to be chemically modified with different elements, such as boron, nitrogen, sulfur, phosphorus, or halogens [30-36].

Graphite oxide represents one of the main precursors of graphene-based nanomaterials. It can be applied as a waste-water purifying agent from inorganic or organic pollutants. It can be synthesized by oxidizing of graphite using permanganates or chlorates in the presence of concentrated acids. The emerging functional groups, such as hydroxyls, epoxides, ketones or carboxylic groups can be easily modified or reduced.[37-45]

Both graphene and graphite oxide have been previously used as an additive in composite materials, such as ceramics-graphene composites [46], silicon nitride [47] or TiO₂-graphene composites [48].

In the construction industry, the materials doped by graphene and graphite oxide are developing quite quickly. Due to their specific properties, they are being studied very thoroughly, because of the impact of their addition in building materials, namely the positive effect on the mechanical resistance and durability [49].

The results presented in previous studies demonstrate some promising results in use with MOC-based composite materials [50, 51]. The combination of the specific properties of both MOC and the carbon-based nanomaterial could make the composite material sufficient or even a superior alternative to construction materials, which are nowadays used more commonly. Their application potential is mostly in extreme conditions, where the commonly used construction materials are not sufficient.

In this contribution, the MOC-based composites containing graphene and graphite oxide were synthesized. The phase composition, morphology and mechanical properties were analyzed and compared to a reference

sample, which did not contain any carbon-based nano-additive. Also, the electrical properties were examined by the use of impedance spectroscopy (IS). From the experimental results was estimated dispersion model of the transport of electric charge in researched materials.

EXPERIMENTAL

Materials

The graphite oxide (GO) was obtained from ACS Material, LLC, United State of America. The graphene (G) nanoplatelets (obtained from Alfa Aesar) had a surface area 500 m²·g⁻¹. Its purity was determined by XRF. The results showed 99.9 wt. % purity with only small traces of S, Si and Fe. The light-burnt magnesia powder was obtained from Styromagnesit-Steirische-Magnesitindustrie Ltd., Austria. Its chemical composition was also analyzed using XRF and recalculated to the content of oxides. The sample contained oxides of magnesium, silicon, calcium, and others. The contents of the oxides are shown in Table 1. The magnesium chloride hexahydrate crystals of p.a. purity (supplied by Lach-Ner Ltd., Czech Republic) were used.

Table 1. Chemical composition of magnesia powder.

| Content | MgO | SiO ₂ | CaO | Al ₂ O ₃ | Fe ₂ O ₃ | SO ₃ |
|---------|------|------------------|-----|--------------------------------|--------------------------------|-----------------|
| % wt. | 80.7 | 4.1 | 5.0 | 5.8 | 3.9 | 0.2 |

Synthetic procedures

The preparation of the composite materials was performed following the standard EN 14016-2 [52]. In our synthetic procedure, the light-burnt magnesia powder was used in excess. This step was taken due to the previous results described in the study of Dong et al., showing the content of active magnesium oxide in the mixture [53]. The mass of the individual raw materials is summarized in Table 2. The preparation process started with the dissolving of MgCl₂·6H₂O in the tap water. The carbon-based nano-additives (graphene powder, graphite oxide powder and their blend) were added in the solution in the amount of 0.5 % by the weight of the magnesium oxychloride binder, creating three samples, which were termed MOC-G (content of graphene powder of 0.5 wt. %), MOC-GO (containing 0.5 wt. %

Table 2. The proportions of the composite mixtures.

| Material | Mass (g) | | | | |
|----------|----------|--------------------------------------|-------|----------|----------------|
| | MgO | MgCl ₂ ·6H ₂ O | Water | Graphene | Graphite oxide |
| MOC | 1918.0 | 849.6 | 564.8 | – | – |
| MOC-G | 1918.0 | 849.6 | 564.8 | 13.8 | – |
| MOC-GO | 1918.0 | 849.6 | 695.0 | – | 13.8 |
| MOC-G+GO | 1918.0 | 849.6 | 564.8 | 6.9 | 6.9 |

of graphite oxide powder), and MOC-G+GO that contained 0.5 wt. % of graphene and graphite oxide powder combined). The magnesia powder was added and dispersed in the magnesium chloride solution. Also, a reference sample, containing only the binder itself was prepared and termed MOC-R. The sample containing GO showed highly hydrophilic behavior resulting in the need to add a higher amount of water compared to the other samples. To get a homogenous suspension of the carbon-based nanomaterials in the solution of magnesium chloride, the mixtures were sonicated for 15 min.

The prepared mixtures were put in the prismatic plastic molds with the dimension of $40 \times 40 \times 160$ mm. After 24 hours the samples were removed from the molds and left for 6 days at laboratory ($T = 22 \pm 2$ °C, RH = 45 ± 5 %).

Analytical techniques

The morphology was studied by SEM (scanning electron microscopy), while the phase composition was analyzed by XRD (X-ray powder diffraction).

The structural parameters such as the bulk density, specific density and open porosity of the hardened composites were investigated. For those purposes, the particular samples were dried in a vacuum drier VacuCell (BT, Czech Republic) at 60 °C. Five samples of each composite mixture were tested. The dry bulk density ρ_b ($\text{kg}\cdot\text{m}^{-3}$) was measured on the halves of casted prisms according to the procedure described in the EN 1015-10 [54]. The expanded combined uncertainty (ECA) of the bulk density test was 1.4 %. The specific density ρ_s ($\text{kg}\cdot\text{m}^{-3}$) was tested by a helium pycnometer Pycnomatic ATC (Porotec, Germany) helium pycnometer. The typical sample mass was about 4 g. The ECA of this experiment was 1.2 %. Based on the dry bulk density and specific density tests, the open porosity ϕ (-) was calculated as originally presented in [55]. The porosity was assessed with the ECA of 2.0 %.

Key parameters affecting the applicability of materials for bearing purposes are mechanical properties. In this paper, flexural strength and compressive strength of the casted composites were determined to reveal the impact of the use of nano-additives in MOC-based matrix. The stiffness of materials was characterized by the modulus of elasticity. The flexural strength of the prepared samples f_f (MPa) was studied on casted prisms in a standard three-point-bending test arrangement. The compressive strength f_c (MPa) was analyzed on the specimen fragments from the flexural strength assessment. Both strength tests were performed in agreement with the EN 1015-11 [56]. The ECA of the strength tests was 1.4 %. The Young's modulus (dynamic modulus of elasticity) E_d (GPa) was determined by the ultrasound velocity test using instrument Pundit Lab+ (Proceq, Schwerzenbach, Switzerland). The ECA of this method was 2.3 %.

The measurement of electrical parameters was conducted with a Solartron SI 1260 Impedance/Gain-Phase Analyzer (Solartron Analytical, UK) with Solartron Dielectric Interface 1296 device. The dependences of the impedance magnitude and the impedance phase on the frequency in the range from 1 to 10 MHz were measured. The dielectric properties can be characterized by the impedance Z (Ω), which is as sum of the resistance R (real part of impedance) and the capacitive reactance $X_C = -1/(\omega C)$ (imaginary part of impedance) as follows

$$Z = R + jX_C = |Z| \exp(j\varphi), \quad (1)$$

where $j = \sqrt{-1}$ is the imaginary unit, $|Z| = \sqrt{R^2 + X_C^2}$ is the impedance modulus and $\varphi = \arctg(X_C/R)$ is the phase shift between a real and an imaginary part [57].

In a case of dispersion of electric charge carriers during transport through the material, the constant phase element (CPE) [58], described by Equation 2, needs to be taken into consideration

$$Z = \frac{1}{Y_0 \omega^n} \exp\left(-\frac{j\pi}{2}n\right). \quad (2)$$

Special cases of this term are capacitive reactance $X_C = -1/(\omega Y_0) = -1/(\omega C)$ (for $n = 1$), resistance $R = -1/Y_0 = 1/G$ (for $n = 0$) or inductive reactance $X_L = \omega/Y_0 = \omega L$ (for $n = -1$). Meaning of parameter Y_0 therefore depends on the type of components (resistance R, conductance G, capacitance C, inductance L, or generally constant phase element CPE).

RESULTS AND DISCUSSION

The prepared samples of MOC-based composite materials containing nano-additives as well as the reference sample are shown in Figure 1.



Figure 1. Photograph of crushed samples of the researched composites.

Using SEM, the microstructure of all four samples was analyzed. The micrographs obtained at lower magnifications are shown in Figure 2. The microstructure

of all the samples presented as highly dense without any visible defects. In addition, more detailed SEM micrographs of the composites can be seen in Figure 3.

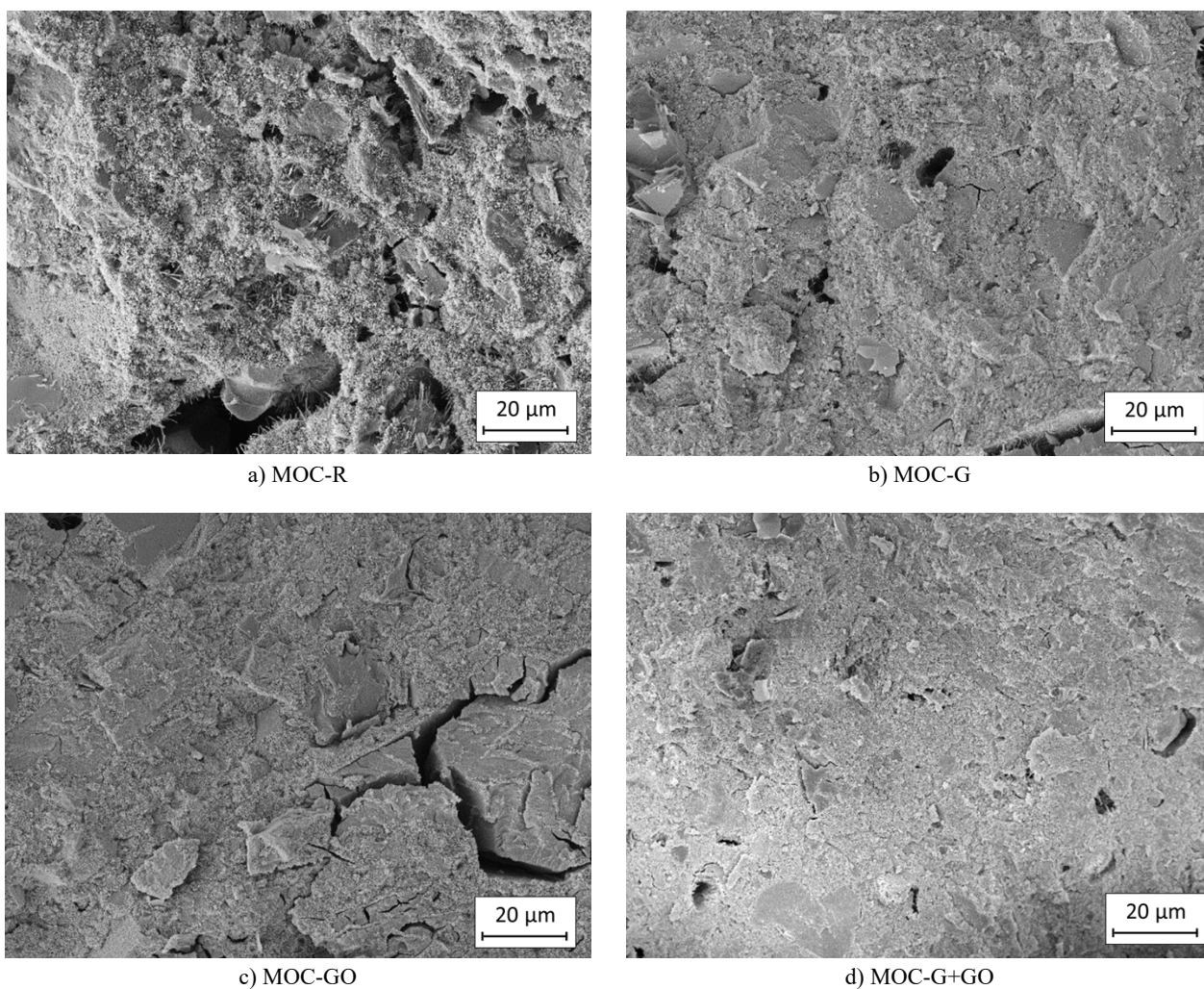


Figure 2. SEM micrographs of the analyzed composites.

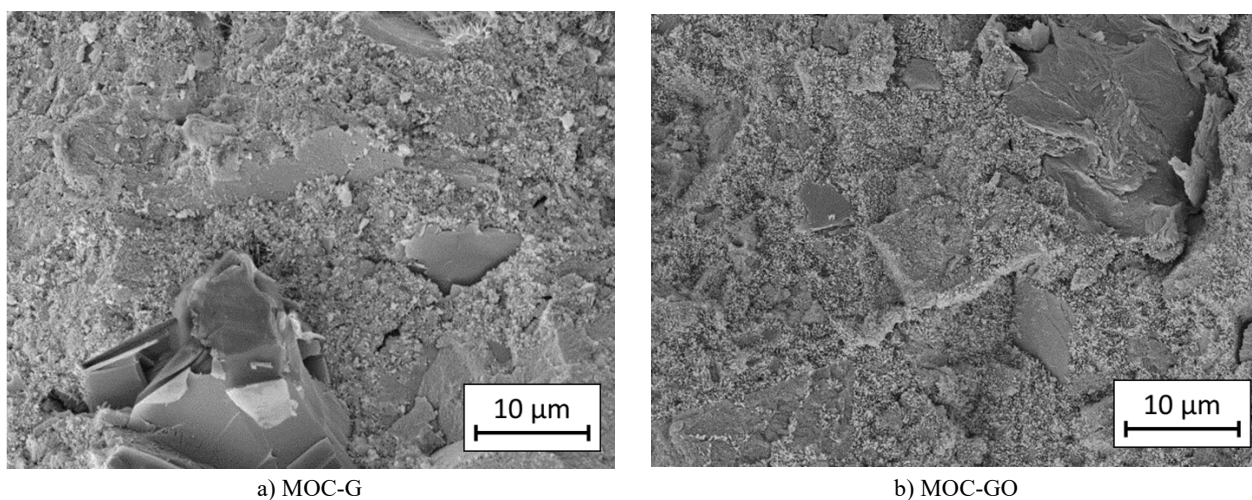
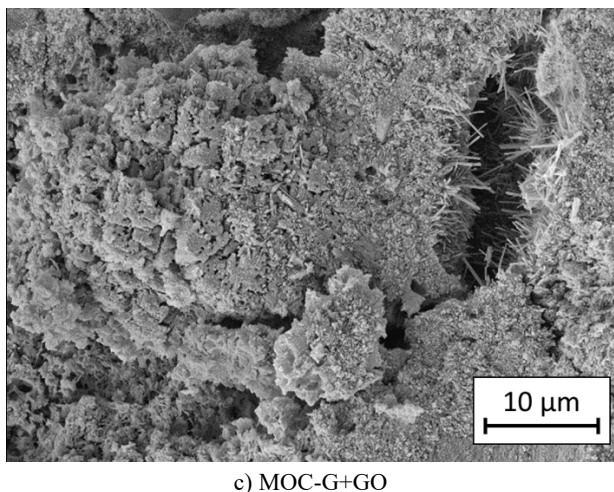


Figure 3. Detailed micrographs of the analyzed composites acquired by SEM. (Continue on next page)



c) MOC-G+GO

Figure 3. Detailed micrographs of the analyzed composites acquired by SEM.

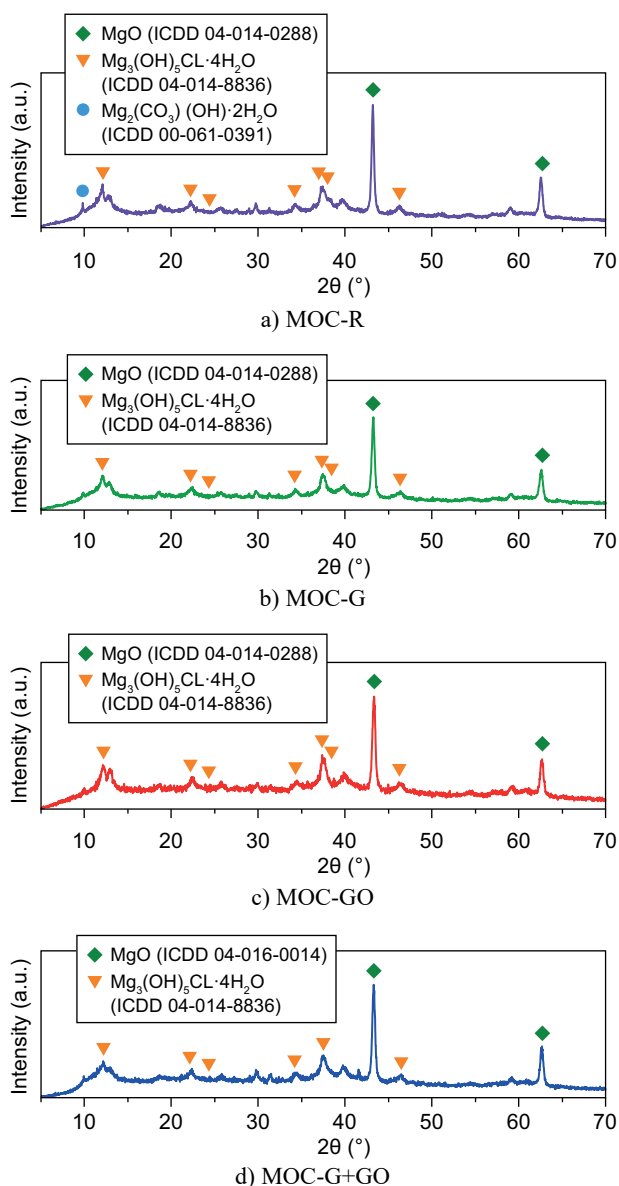


Figure 4. The XRD patterns of the investigated composites.

In the microstructure, there are visible several particle shapes that can be assigned to the various phases. The MgO which is present as a micro-filler is visible as a micro-granular phase. The MOC Phase 5 is present in the form of needle-shaped crystals, which is typical for this sort of materials.

The X-ray diffraction patterns of the samples (see Figure 4) show almost similar phase composition. Both MgO (ICDD 04-014-0288) and $Mg_3(OH)_5Cl \cdot 4H_2O$ (ICDD 04-014-8836, Phase 5 of MOC) are present. The reference sample also shows the presence of chlorartinite (ICDD 00-061-0391), which is present due to the CO_2 -capture process, which is typical for MOC [59]. The nanomaterials cannot be observable in the diffraction patterns due to their fine structure and because only 0.5 wt. % of them were used for the prepared samples.

The basic macrostructural parameters of the MOC-based materials can be seen in Table 3. All tested materials exhibited low open porosity which further dropped with the incorporation of both nano-additives in the composite mix. The lowest porosity yielded the use of graphite oxide, the drop was approx. 45 % in comparison with the reference material labeled MOC. This was assigned to the development of a thin layer of graphite oxide platelets on the precipitated MOC crystals [20]. Qualitatively, the macrostructural data presented in Table 3 were in a good compliance with data provided by SEM that pointed to the highly-dense microstructure of tested materials. Moreover, the needle shape crystals of MOC visible in the detailed SEM micrographs were interlocked with graphene agglomerates and GO platelets which resulted in the decreased porosity of nano-additives modified composites. Except of material MOC-GO, both the bulk density and specific density were almost unaffected by the application of nano-additives in mix composition.

Table 3. The macrostructural parameters of the tested composites.

| Material | ρ_b (kg·m ⁻³) | ρ_s (kg·m ⁻³) | φ (%) |
|----------|--------------------------------|--------------------------------|---------------|
| MOC | 1895 ± 27 | 1970 ± 24 | 3.8 ± 0.1 |
| MOC-G | 1896 ± 27 | 1944 ± 23 | 2.5 ± 0.1 |
| MOC-GO | 1997 ± 28 | 2040 ± 25 | 2.1 ± 0.1 |
| MOC-G+GO | 1900 ± 27 | 1946 ± 23 | 2.4 ± 0.1 |

The mechanical strength and stiffness of MOC-based materials are apparent from Table 4. Except that all composites reported high mechanical strength and elastic modulus which is typical for materials based on MOC [60, 61], two distinct features were observed for nano-additives modified materials. Firstly, the addition of graphene nanoplatelets greatly elevated the compressive strength of MOC-G and MOC-G+GO materials. Then, the use of graphite oxide in mix composition resulted in improved flexural strength and stiffness. Moreover, the synergic performance of nano-additives gave material of enhanced all investigated mechanical parameters.

Table 4. Mechanical parameters of the analyzed composites.

| Material | f_c (MPa) | f_f (MPa) | E_d (GPa) |
|----------|-------------|-------------|-------------|
| MOC | 65.1 ± 0.9 | 16.9 ± 0.2 | 35.6 ± 0.8 |
| MOC-G | 82.1 ± 1.2 | 18.1 ± 0.3 | 36.7 ± 0.8 |
| MOC-GO | 67.6 ± 1.0 | 23.7 ± 0.3 | 40.3 ± 0.9 |
| MOC-G+GO | 76.8 ± 1.1 | 19.8 ± 0.2 | 38.1 ± 0.9 |

In research of supplementary cementitious materials (SCM), assessment of mechanical strength of pozzolan-modified mortars is usually done by strength activity index (SAI) [60]. It is defined in the standard EN 450-1 [62, 63] as a ratio of the compressive strength of the blends with incorporated mineral admixture to the compressive strength of the reference Portland cement mortar. A material is considered as pozzolanic if SAI ≥ 75 %. In this paper, we used the modification of this procedure and evaluated the effectiveness of the tested nano-additives by the strength efficiency coefficient (SEC) which was calculated both for compressive strength (SEC_c) and flexural strength data (SEC_f). The results are introduced in Table 5. For all materials with applied nano-additives the SEC values were > 100 % which clearly demonstrated the contribution of graphene nanoplatelets and graphite oxide to the mechanical resistance of MOC matrix.

Table 5. Strength efficiency coefficient (SEC) of the analyzed composites.

| Composite | SEC_c (%) | SEC_f (%) |
|-----------|-------------|-------------|
| MOC-G | 126.1 | 107.1 |
| MOC-GO | 103.8 | 140.2 |
| MOC-G+GO | 118.0 | 117.2 |

From the measured dependencies of the impedance magnitude and the impedance phase on the frequency, model of the transport of electric charge through the researched materials was proposed (see Figure 5). This model consists from the geometrical capacity C_3 , serial resistivity R_3 , and two parallel combinations of resistors and capacitors (R_1C_1 and R_2C_2) connected in serial. By fitting the parameters of experimental data, the parameters of constant phase element Y and n (see Equation 2) of all model parameters were determined. It was found that

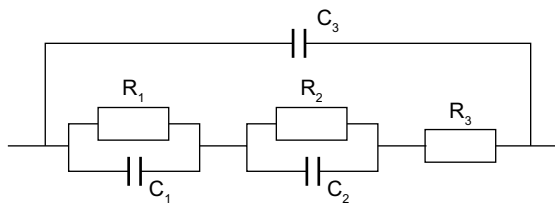


Figure 5. Model of the transport of electric charge in the material determined from the experimental data graphed in Figure 6 (R_3 serial resistivity, C_3 geometrical capacity, R_1, R_2 dispersion volume resistivities, C_1, C_2 dispersion volume capacities).

resistors R_1 and R_2 have dispersion character (dispersion in charge transport) and capacitors C_1 and C_2 are also dispersive (dispersion in charge polarization).

The influence of the model parameters on the experimental data is apparent from the dependences of the impedance phase on the impedance magnitude (see Figure 6). It is evident that volume electric capacity had dispersive character of charge polarization with parameter n_{C1} (see Equation 2) < 1.0 ($n_{C1} \approx 0.97, \varphi_Z \approx -87^\circ$). Also, the volume electric resistivity of electric charge transport exhibited dispersive character ($n_{R1} \approx 0.27, \varphi_Z \approx -25^\circ$).

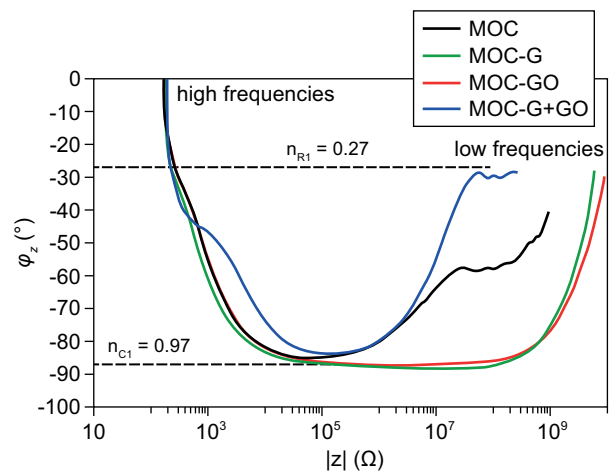


Figure 6. Dependence of impedance phase on its magnitude $\varphi_z = f(|Z|)$ determined from the frequency dependence of both parameters; the dispersion parameters n_{R1} and n_{C1} are introduced for material MOC-GO (dashed lines).

From Figure 6 it is evident the samples MOC-G and MOC-GO changed to resistive character for low frequencies (for impedance magnitudes higher than $10^7 \Omega$), compared to the samples MOC and MOC-G+GO. It was caused by free charges when the only one additive was added (graphene electron transport, graphite oxide hole transport through traps). When the both admixtures were added, the electrons were trapped by the positive states and the conductivity was the same as for pure MOC material.

For better clarity, the structural model characterizing the electric behavior of the studied MOC composites is visualized in Figure 7.

The data of electrical resistivity and capacity calculated using the model presented in Figure 5 is given in Table 6. This data is quite unique as no information on the electrical properties of MOC-based materials is available in literature sources. Due to the addition of graphite oxide, the electrical resistance of material R_1 significantly dropped compared to the reference sample, and the capacity C_1 slightly increased. This was assigned to the formation of GO agglomerates that probably increased the overall conductivity of the composite. As anticipated, the use of highly conductive graphene

led to the reduction of electrical resistivity of MOC-G material. By the addition of graphene, two types of electric charge transport took place, namely the transport in MOC material itself, and in graphene nanoplatelets. In the model, it was expressed by the addition of another resistor (R_2) and capacitor (C_2). However, due to the low concentration of graphene particles, the percolation threshold was not exceeded, and the conductive paths between electrodes were not formed. This was also confirmed by SEM. It was the reason why the composite with graphene exhibited slightly higher electrical resistivity comparison with GO modified material. The electrical capacity of MOC-G composite was greater than that of reference material. The electrical parameters of material MOC-G+GO were affected by the electrical behavior of MOC matrix, GO, and graphene. The conductive effect of graphene was balanced with GO which was caused by the compensation of electric charge carriers of graphene (electrons) and positive bonding centers of GO. In this case, the decrease in porosity contributed to the total conductivity drop. The resistivity of electrodes – contact (R_3) was for all samples negligible. Accordingly, the geometrical capacity (C_3) was for all samples similar and much lower than the capacities of tested materials.

There is necessary to remark, in accordance with the theory of dispersive transport of electrical charge carriers which can be described using constant phase element (CPE) model, the values of electrical resistivity and capacity presented above are valid for angular frequency $\omega = 2\pi f = 1 \text{ rad}\cdot\text{s}^{-1}$ only (see Equation 2).

Although the electrical resistivity of a material defines its capability to withstand the transfer of ions subjected to an electrical field, it can be used for the characterization of the microstructure of examined materials, because it is largely dependent on the microstructural parameters of porous space, such as pore size, shape, tortuosity, and depercolation (discontinuity) [64]. Usually, finer pore network with less interconnectivity gives higher electrical resistivity [65]. However, in our case the differences in porosity were for all tested materials low, thus the main effect on the total electrical conductivity of MOC composites had the properties of used nano-additives themselves and their distribution in the fresh mix and hardened samples. As the result, the low porosity composites exhibited lower electrical resistivity compared to the reference material with the highest porosity.

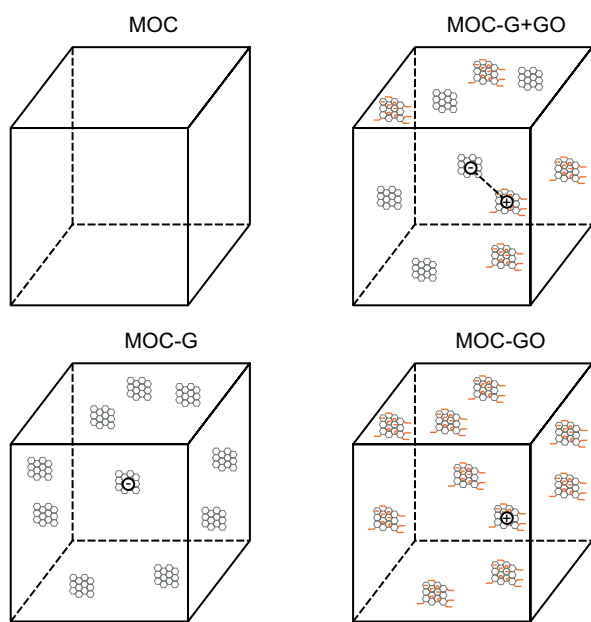


Figure 7. Visualization of MOC composites: nano-additives are scattered in MOC matrix: free charges for MOC-G are electrons (-), free charges for MOC-GO are holes (+), and electrons trapped by positive states for MOC-G+GO are indicated as (-) ---(+).

CONCLUSIONS

Graphene- and graphite oxide-reinforced MOC composites were fabricated and analyzed as prospective materials for the construction industry. Based on the presented results, the following conclusions were reached:

- all the samples had highly dense microstructure without any visible defects;
- various MOC phases such as MgO visible as microgranular phase and MOC Phase 5 needle-shape crystals were detected by SEM;
- the needle shape crystals of MOC were interlocked with graphene agglomerates and GO platelets;
- examined composites exhibited low open porosity which further dropped with the incorporation of both nano-additives in composite mix,
- the open porosity in the 2.1 - 3.8 % range greatly limits permeability of explored materials for moisture transport which thus eliminates moisture induced damage that often prohibits use of MOC materials in wet environments;

Table 6. Electrical parameters of MOC composites.

| Material | R_1 (Ω) | R_2 (Ω) | R_3 (Ω) | C_1 (F) | C_2 (F) | C_3 (F) |
|----------|--------------------|--------------------|--------------------|----------------------|---------------------|----------------------|
| MOC | $5.2 \cdot 10^9$ | – | 625 | $6.0 \cdot 10^{-10}$ | – | $7.0 \cdot 10^{-11}$ |
| MOC-G | $5.0 \cdot 10^8$ | $5.1 \cdot 10^7$ | 800 | $6.0 \cdot 10^{-9}$ | $1.5 \cdot 10^{-9}$ | $7.0 \cdot 10^{-11}$ |
| MOC-GO | $4.2 \cdot 10^8$ | – | 1700 | $7.5 \cdot 10^{-10}$ | – | $4.0 \cdot 10^{-11}$ |
| MOC-G+GO | $6.1 \cdot 10^9$ | – | 700 | $6.5 \cdot 10^{-10}$ | – | $6.8 \cdot 10^{-11}$ |

- the bulk density and specific density remained almost non-affected by the application of nano-additives in mix composition;
- for the evaluation of the contribution of applied reinforcing nano-additives to the mechanical resistance of fabricated composites, the strength efficiency coefficient was newly formulated, its values were for all composites > 100 % which clearly demonstrated the benefits of graphene nanoplatelets and graphite oxide for the enhancement of mechanical resistance of MOC matrix;
- the use graphene nanoplatelets and graphite oxide separately in composite led to the acceleration of transport of electrical charge carriers, on the other hand their combination gave electrical properties similar to those of reference MOC paste.

Acknowledgement

This work was supported by the Czech Science Foundation, grant number 20-01866S and from the grant of Specific university research – grant MSMT no. 20-SVV/2020. The support received from the Brno University of Technology under the project No FCH-S-20-6340 is also greatly acknowledged.

REFERENCES

- Sorel S. (1867). On a new magnesium cement. *CR Acad Sci*, 65(65), 102-104.
- Bilinski H., Matković, B., Mažuranić C., Žunić T. B. (1984): The formation of magnesium oxychloride phases in the systems $MgO-MgCl_2-H_2O$ and $NaOH-MgCl_2-H_2O$. *Journal of the American Ceramic Society*, 67(4), 266-269. doi: 10.1111/j.1151-2916.1984.tb18844.x
- Dinnebier R. E., Freyer D., Bette S., Oestreich M. (2010): $9Mg(OH)_2 \cdot MgCl_2 \cdot 4H_2O$, a high temperature phase of the magnesia binder system. *Inorganic chemistry*, 49 (21), 9770-9776. doi: 10.1021/ic1004566
- Dinnebier R. E., Oestreich M., Bette S., Freyer D. (2012): $2Mg(OH)_2 \cdot MgCl_2 \cdot 2H_2O$ and $2Mg(OH)_2 \cdot MgCl_2 \cdot 4H_2O$, two high temperature phases of the magnesia cement system. *Zeitschrift für anorganische und allgemeine Chemie*, 638 (3-4), 628-633. doi: 10.1002/zaac.201100497
- Feitknecht W., Held F. (1944): Über die Hydroxychloride des Magnesiums. *Helvetica Chimica Acta*, 27(1), 1480-1495. doi: 10.1002/hlca.194402701189
- Walter-Lévy L. (1937): Chlorocarbonate basique de magnésium. *CR Hebd. Séances Acad. Sci*, 204, 1943-1946.
- Walter-Lévy L., de Wolff P. M. (1949): Contribution A Letude Du Ciment Sorel. C. R. Hebd, Séances Acad. Sci. 229, 1077-1079.
- Hendriks C. A., Worrell E., De Jager D., Blok K., Riemer P. (1998). Emission reduction of greenhouse gases from the cement industry. In: *Proceedings of the fourth international conference on greenhouse gas control technologies*. Interlaken, Austria, IEA GHG R&D Programme, pp. 939-944. <http://geomimicry.net/files/sustainability%20documents/EmissionReductionofGreenhouseGasesfromtheCementIndustry.pdf>
- Imbabi M. S., Carrigan C., McKenna S. (2012): Trends and developments in green cement and concrete technology. *International Journal of Sustainable Built Environment*, 1(2), 194-216. doi: 10.1016/j.ijse.2013.05.001
- Naik T. R. (2008): Sustainability of concrete construction. *Practice Periodical on Structural Design and Construction*, 13(2), 98-103. Doi: 10.1061/(ASCE)1084-0680(2008)13:2(98)
- Thompson H. C. (1976). *Fireproof product using magnesium oxychloride cement*, Google Patents.
- Li G., Yu Y., Li J., Wang Y., Liu H. (2003): Experimental study on urban refuse/magnesium oxychloride cement compound floor tile. *Cement and Concrete Research*, 33(10), 1663-1668. doi: 10.1016/S0008-8846(03)00136-4
- Plekhanova T., Keriene J., Gailius A., Yakovlev G. (2007): Structural, physical and mechanical properties of modified wood–magnesia composite. *Construction and Building Materials*, 21(9), 1833-1838. doi: 10.1016/j.conbuildmat.2006.06.029
- Sorre C. A., Armstrong C. R. (1976): Reactions and Equilibria in magnesium Oxychloride cements. *Journal of the American Ceramic Society*, 59(1-2), 51-54. doi: 10.1111/j.1151-2916.1976.tb09387.x
- Cole, W. F., & Demediuk, T. (1955). X-ray, thermal, and dehydration studies on magnesium oxychlorides. *Australian Journal of Chemistry*, 8(2), 234-251. doi: 10.1071/CH9550234
- Jankovsky O., Bartunek V., Antoncik F., Jirickova A., Lauermannova A.-M., et al. (2019): Wood chips ash processing and its utilization in magnesium phosphate cement composites. *Ceram. Silikáty*, 63, 267-276. doi: 10.13168/cs.2019.0020
- Kurdowski W. (2014). Special cements. In *Cement and Concrete Chemistry*. Springer, Dordrecht. p.603-659. doi: 10.1007/978-94-007-7945-7_9
- Li C., Yu H. (2010): Influence of fly ash and silica fume on water-resistant property of magnesium oxychloride cement. *Journal of Wuhan University of Technology-Mater. Sci. Ed.*, 25(4), 721-724. doi: 10.1007/s11595-010-0079-y
- Zhang C., Deng D. (1995): Research on the water resistance of magnesium oxychloride cement and its improvement. *Journal-Chinese Ceramic Society*, 23, 673-679.
- Jankovský O., Lojka M., Lauermannová A.-M., Antončík F., Pavlíková M., Záleská M., Pavlík Z., Pivák A. et al. (2020): Towards novel building materials: High-strength nanocomposites based on graphene, graphite oxide and magnesium oxychloride. *Applied Materials Today*, 20, 100766. doi: 10.1016/j.apmt.2020.100766
- Geim A. K., Novoselov K. S. (2007): The rise of graphene. *Nature materials*, 6, 183-191. doi: 10.1038/nmat1849
- Chen J.-H., Jang C., Xiao S., Ishigami M., Fuhrer M. S. (2008): Intrinsic and extrinsic performance limits of graphene devices on SiO_2 . *Nature Nanotechnology*, 3(4), 206-209. doi: 10.1038/nnano.2008.58
- Novoselov K. S., Geim A. K., Morozov S. V., Jiang D., Zhang Y., Dubonos S. V., et al. (2004): Electric field effect in atomically thin carbon films. *Science*, 306(5696), 666-669. doi: 10.1126/science.1102896
- Sofer Z., Šimek P., Jankovský O., Sedmidubský D., Beran P., Pumera M. (2014): Neutron diffraction as a precise and reliable method for obtaining structural properties of bulk

- quantities of graphene. *Nanoscale*, 6(21), 13082-13089. doi: 10.1039/C4NR04644G
25. Popov V. N. (2004): Carbon nanotubes: properties and application. *Materials Science and Engineering: R: Reports*, 43(3), 61-102. doi: 10.1016/j.msre.2003.10.001
 26. Terrones M., Botello-Méndez A. R., Campos-Delgado J., López-Urías F., Vega-Cantú Y. I., Rodríguez-Macias F. J., et al. (2010): Graphene and graphite nanoribbons: Morphology, properties, synthesis, defects and applications. *Nano Today*, 5(4), 351-372. doi: 10.1016/j.nantod.2010.06.010
 27. Yadav B., Kumar R. (2008): Structure, properties and applications of fullerenes. *International Journal of Nanotechnology and Applications*, 2, 15-24.
 28. Neto A. C., Guinea F., Peres N., Novoselov K. S., Geim A. K. (2009): The electronic properties of graphene. *Reviews of modern physics*, 81(1), 109. doi: 10.1103/RevModPhys.81.109
 29. Pereira V. M., Guinea F., Dos Santos J. L., Peres N., Neto A. C. (2006): Disorder induced localized states in graphene. *Physical Review Letters*, 96(3), 036801. doi: 10.1103/PhysRevLett.96.036801
 30. Bouša D., Luxa J., Mazanek V., Jankovský O., Sedmidubský D., Klimova K., Pumera M., Sofer Z. (2016): Toward graphene chloride: chlorination of graphene and graphene oxide. *RSC Advances*, 6(71), 66884-66892. doi: 10.1039/C6RA14845J
 31. Jankovský O., Kučková Š. H., Pumera M., Šimek P., Sedmidubský D., Sofer Z. (2014): Carbon fragments are ripped off from graphite oxide sheets during their thermal reduction. *New Journal of Chemistry*, 38(12), 5700-5705. doi: 10.1039/C4NJ00871E
 32. Panchakarla L., Subrahmanyam K., Saha S., Govindaraj A., Krishnamurthy H., Waghmare U., Rao C. (2009): Synthesis, structure, and properties of boron-and nitrogen-doped graphene. *Advanced Materials*, 21(46), 4726-4730. doi: 10.1002/adma.200901285
 33. Qu L., Liu Y., Baek J.-B., Dai L. (2010): Nitrogen-doped graphene as efficient metal-free electrocatalyst for oxygen reduction in fuel cells. *ACS Nano*, 4, 1321-1326.
 34. Wu J., Xie L., Li Y., Wang H., Ouyang Y., Guo J., Dai H. (2011): Controlled chlorine plasma reaction for noninvasive graphene doping. *Journal of the American Chemical Society*, 133(49), 19668-19671. doi: 10.1021/ja2091068
 35. Yang Z., Yao Z., Li G., Fang G., Ni, H., Liu Z., et al. (2012): Sulfur-doped graphene as an efficient metal-free cathode catalyst for oxygen reduction. *ACS Nano*, 6(1), 205-211. doi: 10.1021/nn203393d
 36. Zhang C., Mahmood N., Yin H., Liu F., Hou Y. (2013): Synthesis of phosphorus-doped graphene and its multifunctional applications for oxygen reduction reaction and lithium ion batteries. *Advanced Materials*, 25(35), 4932-4937. doi: 10.1002/adma.201301870
 37. Fonseca B., Figueiredo H., Rodrigues J., Queiroz A., Tavares T. (2011): Mobility of Cr, Pb, Cd, Cu and Zn in a loamy sand soil: A comparative study. *Geoderma*, 164(3-4), 232-237. doi: 10.1016/j.geoderma.2011.06.016
 38. Gopal K., Srivastava S. B., Shukla S., Bersillon J. L. (2004): Contaminants in drinking water and its mitigation using suitable adsorbents: an overview. *Journal of Environmental Biology*, 25(4), 469-475.
 39. Jankovský O., Šimek P., Klímová K., Sedmidubský D., Pumera M., Sofer Z. (2015): Highly selective removal of Ga³⁺ ions from Al³⁺/Ga³⁺ mixtures using graphite oxide. *Carbon*, 89, 121-129. doi: 10.1016/j.carbon.2015.03.025
 40. Kołodzyńska D., Krukowska J. A., Thomas P. (2017): Comparison of sorption and desorption studies of heavy metal ions from biochar and commercial active carbon. *Chemical Engineering Journal*, 307, 353-363. doi: 10.1016/j.cej.2016.08.088
 41. Kyzas G. Z., Deliyanni E. A., Matis K. A. (2014): Graphene oxide and its application as an adsorbent for wastewater treatment. *Journal of Chemical Technology & Biotechnology*, 89(2), 196-205. doi: 10.1002/jctb.4220
 42. Lu C., Chiu H. (2008). Chemical modification of multiwalled carbon nanotubes for sorption of Zn²⁺ from aqueous solution. *Chemical Engineering Journal*, 139(3), 462-468. doi: 10.1016/j.cej.2007.08.013
 43. Sitko R., Turek E., Zawisza B., Malicka E., Talik E., Heimann, J., et al. (2013): Adsorption of divalent metal ions from aqueous solutions using graphene oxide. *Dalton transactions*, 42(16), 5682-5689. doi: 10.1039/C3DT33097D
 44. Tan X. L., Fang M., Chen C. L., Yu S. M., Wang X. K. (2008): Counterion effects of nickel and sodium dodecylbenzene sulfonate adsorption to multiwalled carbon nanotubes in aqueous solution. *Carbon*, 46, 1741-1750. doi: 10.1016/j.carbon.2008.07.023
 45. Zhao Z. Q., Chen X., Yang Q., Liu J. H., Huang X. J. (2012): Selective adsorption toward toxic metal ions results in selective response: electrochemical studies on a polypyrrole/reduced graphene oxide nanocomposite. *Chemical Communications*, 48(16), 2180-2182. doi: 10.1039/C1CC16735A
 46. Jiang Z., Wang J., Meng L., Huang Y., Liu L. (2011): A highly efficient chemical sensor material for ethanol: Al₂O₃/Graphene nanocomposites fabricated from graphene oxide. *Chemical Communications*, 47(22), 6350-6352. doi: 10.1039/C1CC11711D
 47. Walker L. S., Marotto V. R., Rafiee M. A., Koratkar N., Corral E. L. (2011): Toughening in graphene ceramic composites. *ACS Nano*, 5(4), 3182-3190. doi: 10.1021/nn200319d
 48. Williams G., Seger B., Kamat P. V. (2008): TiO₂-graphene nanocomposites. UV-assisted photocatalytic reduction of graphene oxide. *ACS nano*, 2(7), 1487-1491. doi: 10.1021/nn800251f
 49. Compton O. C., Nguyen S. T. (2010): Graphene oxide, highly reduced graphene oxide, and graphene: versatile building blocks for carbon-based materials. *Small*, 6(6), 711-723. doi: 10.1002/smll.200901934
 50. Amin M., Putra N., Kosasih E. A., Prawiro E., Luanto R. A., Mahlia T. M. I. (2017): Thermal properties of beeswax/graphene phase change material as energy storage for building applications. *Applied Thermal Engineering*, 112, 273-280. doi: 10.1016/j.applthermaleng.2016.10.085
 51. Horszczaruk E., Mijowska E., Kalenczuk R. J., Aleksandrak M., Mijowska S. (2015): Nanocomposite of cement/graphene oxide—Impact on hydration kinetics and Young's modulus. *Construction and Building Materials*, 78, 234-242. doi: 10.1016/j.conbuildmat.2014.12.009
 52. Tang S., Hu Y., Ren W., Yu P., Huang Q., Qi X., et al. (2019). Modeling on the hydration and leaching of eco-friendly magnesium oxychloride cement paste at the micro-scale. *Construction and Building Materials*, 204, 684-690. doi: 10.1016/j.conbuildmat.2019.01.232

53. Dong J. M., Yu H. F., Zhang L. M. (2010): Study on experimental conditions of hydration methods of determining active magnesium oxide content. *Journal of Salt Lake Research*, 18(1), 38-41.
54. EN 1015-10 (1999). Methods of Test for Mortar for Masonry – Part 10: Determination of Dry Bulk Density of Hardened 676 Mortar, ed., European Committee for Standardization, Brussels, Belgium.
55. Jankovsky O., Pavlíková M., Sedmidubsky D., Bouša D., Lojka M., Pokorný J., Záleská M., Pavlík Z. (2017): Study on pozzolana activity of wheat straw ash as potential admixture for blended cements. *Ceramics-Silikáty*, 61, 327-339. doi: 10.13168/cs.2017.0032
56. Hall D. A., Stevens R., El-Jazairi B. (2001): The effect of retarders on the microstructure and mechanical properties of magnesia-phosphate cement mortar. *Cement and Concrete Research*, 31(3), 455-465. doi: 10.1016/S0008-8846(00)00501-9
57. Macdonald J. R., Barsoukov E. (2005): Impedance spectroscopy: theory, experiment, and applications. *History*, 1(8), 1-13.
58. Kochowski S., Nitsch K. (2002): Description of the frequency behaviour of metal-SiO₂-GaAs structure characteristics by electrical equivalent circuit with constant phase element. *Thin Solid Films*, 415(1-2), 133-137. doi: 10.1016/S0040-6090(02)00506-0
59. Jankovský O., Lojka M., Lauermannová A. M., Antončík F., Pavlíková M., Pavlík Z., Sedmidubský D. (2020): Carbon Dioxide Uptake by MOC-Based Materials. *Applied Sciences*, 10(7), 2254. doi: 10.3390/app10072254
60. EN 1015-11 (1999). Methods of Test for Mortar for Masonry – Part 10: Determination of Flexural and Compressive Strength 678 of Hardened Mortar, ed., European Committee for Standardization, Brussels, Belgium.
61. Misra A. K., Mathur R. (2007): Magnesium oxychloride cement concrete. *Bulletin of Materials Science*, 30(3), 239-246. doi: 10.1007/s12034-007-0043-4
62. Thorstensen R. T., Fidjestol P. (2015): Inconsistencies in the pozzolanic strength activity index (SAI) for silica fume according to EN and ASTM. *Materials and Structures*, 48(12), 3979-3990. doi: 10.1617/s11527-014-0457-6
63. EN 450-1 (2012). Fly ash for concrete – Part 1: Definition, specifications and conformity criteria, European Committee for Standardization, ed., Brussels.
64. Lee S. W., Lee T. H., Park J. W., Park C. H., Kim H. J., Kim S. M., et al. (2015): The effect of laser irradiation on peel strength of temporary adhesives for wafer bonding. *International Journal of Adhesion and Adhesives*, 57, 9-12. doi: 10.1016/j.ijadhadh.2014.09.002
65. Hornbostel K., Larsen C. K., Geiker, M. R. (2013): Relationship between concrete resistivity and corrosion rate – A literature review. *Cement and Concrete Composites*, 39, 60-72. doi: 10.1016/j.cemconcomp.2013.03.019